# Joule Heating Effects in MHD Generator Boundary Layers

R. Kent James* and Charles H. Kruger†
*Stanford University, Stanford, California*

**Experimental measurements were performed of temperature and electron number density profiles on a laboratory-scale MHD generator. Comparisons between calculations from a two-dimensional theory and measurements for cases without current generally showed good agreement when the turbulence model properly accounted for the effects of freestream turbulence, although small discrepancies were observed between theory and experiments for the overall profile shape. Comparisons of experimental temperature profiles without current to profiles with current showed a marked temperature increase in the boundary layer due to Joule heating. The magnitude of the increase was well predicted by the two-dimensional boundary-layer theory. Measured temperature profiles with current and magnetic field did not agree with predictions. The predicted profile in the inner region of the boundary layer for a case with current and magnetic field was above a similar case without current, whereas measurements for anode boundary layers were below control profiles without current. A cathode boundary layer behaved oppositely to the anode boundary layers. Three-dimensional recirculation induced by nonuniformities in axial current could explain the discrepancies.**

## Nomenclature

$B$ = magnetic field intensity
$c$ = speed of light
$e$ = electron charge
$h$ = Plank's constant; also stagnation enthalpy
$J$ = current density
$k$ = Boltzmann's constant
$l$ = half the distance between opposing electrodes
$m_e$ = electron mass
$N_e$ = electron number density
$p$ = pressure
$Pr$ = Prandtl number
$q$ = heat flux
$Re$ = Reynolds number
$\dot{R}_e$ = electron recombination rate
$u,v,w$ = velocity components in the $x$, $y$, and $z$ directions, respectively
$x,y,z$ = orthogonal coordinates
$\alpha$ = electron recombination rate coefficient
$\delta_1$ = boundary-layer displacement thickness
$\lambda$ = wavelength
$\mu$ = viscosity
$\mu_e$ = electron mobility
$\mu_i$ = ion mobility
$\rho$ = density
$\sigma$ = electrical conductivity; also Stefan-Boltzmann constant

## Introduction

MAGNETOHYDRODYNAMIC (MHD) electric power generation is being vigorously developed as an alternative to presently used forms of energy conversion, as MHD generators are expected to provide a substantial improvement in the efficiency of electric power generation. Many loss mechanisms which significantly affect the generator performance occur in the electrode wall boundary layer of an MHD generator, for example, electrode voltage drop, heat transfer, axial leakage, and axial breakdown. While in many ways the electrode wall boundary layer is similar to extensively studied boundary layers in applications such as turbine blades or rocket nozzles, unique effects can occur in the electrode wall boundary layer which have not been extensively studied. In the present work, the role of these effects is assessed by performing experimental measurements of temperature profiles in a small-scale MHD generator, and comparing these profiles to predictions from a two-dimensional numerical model of the electrode wall boundary layer.

Early theoretical work on the gasdynamic aspects of MHD generators was done by Kerrebrock and co-workers in the early 1960s. They developed solutions for insulator and electrode wall boundary layers for a restricted set of laminar MHD flows.[1,2] After the development of finite difference methods for the solution of boundary-layer equations in the late 1960s, several papers appeared that used these methods to solve MHD boundary-layer flows.[3-10] These computations demonstrated that electron recombination kinetics, electron temperature nonequilibrium, and Joule heating can be important in the electrode wall boundary layer, and that $J \times B$ effects can be important in the insulating wall boundary layer.

Although some comparisons of the existing models to experiments have been made, generally the limits of the models have not been established. Parameters which govern the models, such as turbulence parameters and kinetic constants, are not well established for MHD conditions. Uncertainties exist in the modeling of physical phenomena such as three-dimensional effects, nonuniformities, turbulence damping, and MHD-driven instabilities. With these unknowns, it is important that the theoretical models be compared to experiments before placing excessive confidence in the theoretical results.

Experimental boundary-layer research in combustion MHD generators has been more limited than theoretical research. Experimental verification of the role of the thermal boundary layer in determining electrode voltage drops was provided by Kessler.[11] Measurements of turbulent boundary-layer profiles in combustion MHD generators have been made by Daily,[8] Kirillov et al.,[12] and Rankin,[9] but no measurements of the thermal boundary-layer profiles in a combustion MHD generator have been made under conditions where the boundary layer was noticeably affected by the current interactions. Particularly lacking are experimental data for plasma profiles measured under conditions where current interactions are important.

Received Oct. 10, 1981; revision received July 9, 1982. Copyright © American Institute of Aeronautics and Astronautics, Inc., 1982. All rights reserved.

*High Temperature Gasdynamics Laboratory; presently Process Improvement Engineer, Energy and Environment R&D, Weyerhaeuser Co., Tacoma, Wash. Member AIAA.

†Professor and Chairman, Department of Mechanical Engineering, High Temperature Gasdynamics Laboratory. Member AIAA.

## Theory

A comparison of the measurements to theoretical calculations is desirable to interpret the experiments. For this purpose, theoretical calculations were performed using a computer program originally developed by Daily.[8] This programs solves the two-dimensional boundary-layer equations for the electrode wall boundary layer, including MHD terms. The model utilized in the program is subject to the following assumptions:

1) The electrodes operate in the diffuse mode of current transport.

2) The boundary-layer equations are considered to be averaged over an electrode-insulator cycle, so that no account is taken of the variation of fluid properties within an electrode-insulator cycle.

3) Radiation heat transfer from the gas is neglected.

4) Variations in pressure are considered only in the axial direction.

5) Near-electrode phenomena associated with cathodes are ignored.

6) Fluctuations of MHD terms and of density are ignored in the time-averaging of the boundary-layer equations.

7) Chemical equilibrium is assumed for all species except electrons and ions.

All of these assumptions are felt to be reasonable for the conditions of the experiments.

The equations used in the boundary-layer model are summarized below. Figure 1 describes the coordinate system used in the equations. Further details of the theory are available in James.[13]

### Conservation Equations

Continuity:

$$\frac{\partial \rho u}{\partial x}+\frac{\partial \rho v}{\partial y}+\frac{\partial \rho w}{\partial z}=0 \tag{1a}$$

Momentum:

$$\rho u\frac{\partial u}{\partial x}+\rho v\frac{\partial u}{\partial y}=\frac{\partial}{\partial y}\left[(\mu+\rho\epsilon_m)\frac{\partial u}{\partial y}\right]-\frac{\partial p}{\partial x}+J_yB_z \tag{1b}$$

Energy:

$$\rho u\frac{\partial h}{\partial x}+\rho v\frac{\partial h}{\partial y}=\frac{\partial}{\partial y}\left[\left(\frac{\mu}{Pr}+\rho\epsilon_D\right)\frac{\partial h}{\partial y}\right]$$

$$+\frac{1}{2}\frac{\partial}{\partial y}\left[(\mu+\rho\epsilon_m)\left(1-\frac{1}{Pr}\right)\frac{\partial u^2}{\partial y}\right]+\frac{J^2}{\sigma}+J_yuB_z \tag{1c}$$

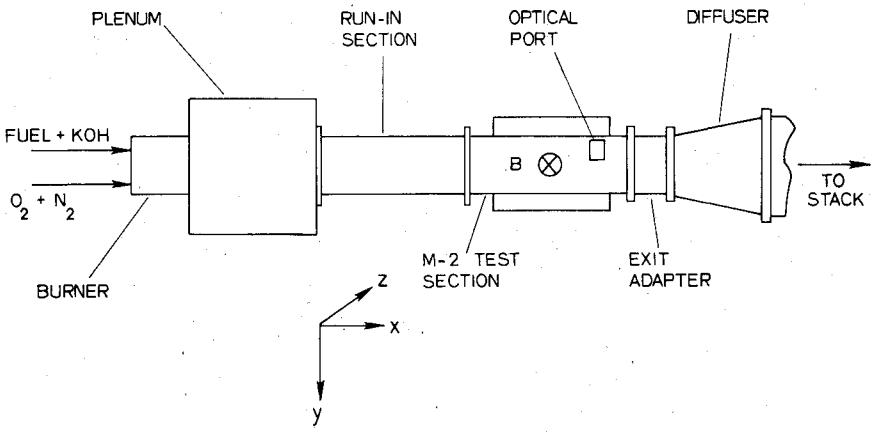


**Fig. 1 Schematic of the flow train used in the experimental measurements.**

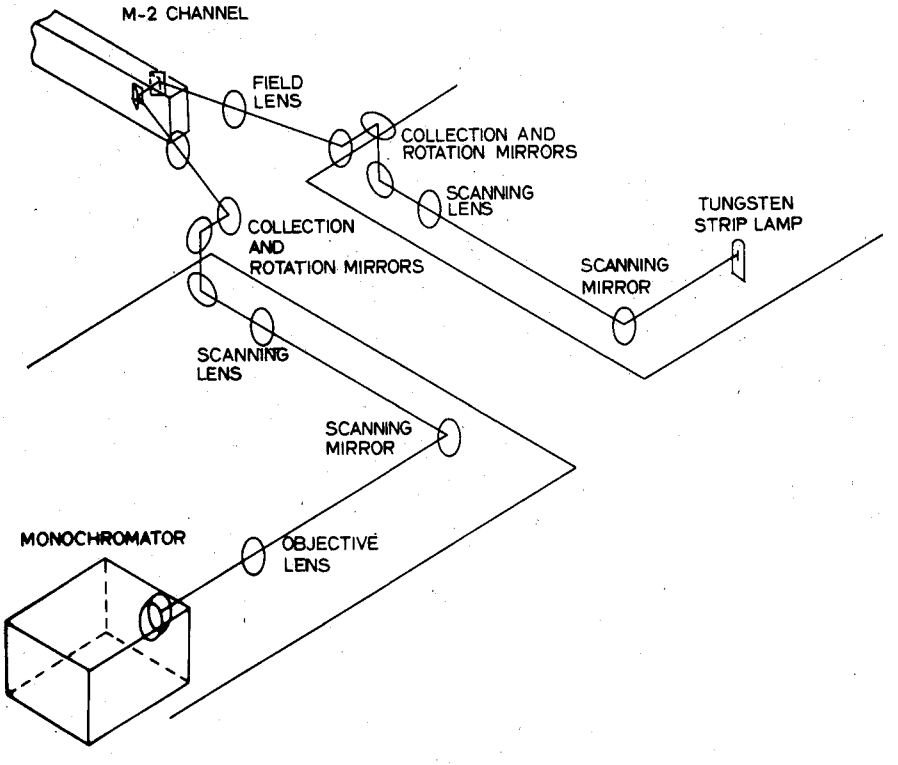


**Fig. 2 Schematic of the optical setup used in the IBL series of experiments.**

Ambipolar Diffusion:

$$\rho u \frac{\partial C_e}{\partial x} + \rho v \frac{\partial C_e}{\partial y} = \frac{\partial}{\partial y}\left[\rho (D_a + \epsilon_D) \frac{\partial C_e}{\partial y}\right] + \dot{R}_e \tag{1d}$$

Here $D_a$ is the ambipolar diffusion coefficient, $\epsilon_m$ and $\epsilon_D$ the eddy diffusivities for momentum and diffusion equations, respectively, $h$ the stagnation enthalpy, and $C_e$ the electron mass fraction. Note that all dependent variables in these equations are time-averaged quantities.

**Boundary Conditions**

For $y=0$:

$$u=v=0, \quad C_e = C_e^*(T_w)$$

$$q_c = -\frac{\mu}{Pr}\frac{\partial h}{\partial y}, \quad q_w = H(T_0 - T_w) = q_c + q_R \tag{2a}$$

Here $C_e^*(T_w)$ is the equilibrium value of the electron concentration at temperature $T_w$, $H$ a heat-transfer conductance to a coolant at temperature $T_0$, $q_R$ the radiation heat flux to the wall, and $q_c$ the convective heat flux.

For $y=\ell$:

$$\frac{\partial u}{\partial y} = v = \frac{\partial h}{\partial y} = \frac{\partial C_e}{\partial y} = 0 \tag{2b}$$

**Initial Conditions**

Initial conditions for velocity ae obtained using a three-layer turbulent model similar to that used by Martinelli.[14] The enthalpy profile is assumed to be similar to the velocity profile. $N_e$ is initialized using the equilibrium $N_e$ values from the initial temperature profile. The initial conditions are typically applied sufficiently far upstream such that the initial profile shapes do not have a significant impact on the desired results from the two-dimensional model.

**Turbulence Closure**

The turbulence closure model used is a mixing-length type described by Crawford and Kays.[15] Important turbulence parameters from that model include $\kappa$ (the von Kármán constant) and $A_0^+$ (the dimensionless sublayer thickness). For duct flows, the model specifies that the eddy diffusivities in the outer regions of the boundary layer for momentum and for other variables ($\epsilon_m$ and $\epsilon_D$, respectively) are given by the expressions

$$\epsilon_m = \nu A_c (Re_{Hy})^{B_c} \tag{3a}$$

$$\epsilon_D = \epsilon_m Pr_t^{-1} \tag{3b}$$

where $Re_{Hy}$ is the channel hydraulic diameter Reynolds number, $Pr_t$ the turbulent Prandtl number, and $A_c$ and $B_c$ adjustable parameters. Recommended values of $A_c$ and $B_c$ are $A_c = 0.005$ and $B_c = 0.9$.[15]

**Wall Radiation Model**

The effect of wall radiation from the hot sidewalls to the cool electrode wall is modeled in an approximate manner. The radiation heat flux $q_R$ is calculated based on the difference between the electrode wall temperature $T_w$ and an average temperature $T_a$ of the surfaces facing the electrode wall,

$$q_R = \sigma\epsilon (T_w^4 - T_a^4) \tag{4}$$

where $\sigma$ is the Stefan-Boltzmann constant and $\epsilon$ the electrode wall emissivity. In the calculations for the conditions of this work, $\epsilon = 0.5$ and $T_a = 2000$ K.

**Recombination Coefficient**

The recombination rate $\dot{R}_e$ is given by

$$\dot{R}_e = m_e \alpha (N_e^{*2} - N_e^2) \tag{5}$$

where $N_e^*$ refers to equilibrium $N_e$. The recombination coefficient $\alpha$ is calculated using the Hinnov-Hirschberg formula[16] for three-body electron-ion collisions, and cross sections of Kelley and Padley[17] for molecular collisions, resulting in

$$\alpha = 1.08.10^{-20} N_e T^{-9/2} + 2.60.10^{-3} p T^{-2} \text{ (m·kg·s units)} \tag{6}$$

**Properties**

Calculations of transport and thermodynamic properties were made using the program EQUIL. The program was originally developed by Pepper[18] and has undergone further development at the High Temperature Gasdynamics Laboratory. The program EQUIL calculates the equilibrium gas composition and properties based on this composition. The conductivity calculation uses the Frost mixture rule, uses cross sections obtained from Spencer and Phelps[19] and includes the effect of electron attachment to negative ions.

The ambipolar diffusion coefficient is expressed in terms of mobility by[20]

$$D_a = \frac{2kT}{e} \frac{\mu_e \mu_i}{(\mu_e + \mu_i)} \tag{7}$$

The value of $\mu_i$ used was obtained from a calculation by Clement.[21]

**Core Solution**

The pressure in the channel is determined by solving the core gasdynamic equations, and a core continuity equation of the form,

$$\frac{\mathrm{d}}{\mathrm{d}x}(\rho_\infty u_\infty A_e) = 0 \tag{8}$$

The effective cross-sectional area $A_e$ is approximated by

$$A_e = 4(w - \delta_{l,s})(\ell - \delta_{l,e}) \tag{9}$$

where $w$ and $\ell$ are the channel half-widths perpendicular to the sidewall and electrode wall, and $\delta_{l,s}$ and $\delta_{l,e}$ are the sidewall boundary layer and electrode boundary-layer displacement thicknesses. When needed, $\delta_{l,s}$ is calculated using a simple integral model of the sidewall boundary layer.

**Electrical Solution**

The boundary-layer equations require specification of $J^2$ as a function of $x$ and $y$, and $J_y$ as a function of $x$. These functions are provided by using an external program to calculate a nondimensional streamline solution using a conductivity variation calculated by the boundary-layer model for a typical condition without current. The equations used in the streamline calculation follow Oliver.[22] After obtaining a nondimensional streamline solution, the value of nondimensional $J^2$ is averaged over an electrode-insulator cycle to give a nondimensional $J^2(y)$. At each $x$ location in the boundary-layer program marching procedure, the dimensional values of $J_y$ and $J^2(y)$ are specified based on the average current value in the experimental condition being modeled.

**Numerical Method**

The numerical method used is similar to that used in STAN5.[15] The method consists of transforming the governing partial differential equations into dimensionless stream

function coordinates and approximating the resulting equations with linearized finite difference equations. Further details are discussed by Daily.[8]

## Description of Experimental Work

The experimental data consist of spectroscopic measurements of temperature profiles under varying conditions in the electrode wall boundary layer of the Stanford M-2 MHD generator. The data were taken in two major experimental series, denoted ABL (applied field boundary layer) and IBL (induced field boundary layer). The ABL series was conducted with an applied electric field from battery banks and no magnetic field. The IBL series was conducted in a magnetic field, with batteries used to augment the Faraday current.

### Hardware Description

The experiments were conducted in the Stanford M-2 MHD facility.[23] An overall schematic of the flow train is shown in Fig. 1. The basic combustion system consisted of a swirl-stabilized ethanol-burning combustor, which fed into an MgO-lined plenum chamber and then into a subsonic nozzle. The ethanol was burned with a stoichiometric amount of oxygen, with nitrogen added to control the temperature. Potassium seed to enhance the electrical conductivity of the combustion products was added to the plasma by dissolving potassium hydroxide pellets in the ethanol fuel prior to the experiments in the ratio 7 kg of KOH per 100 kg of ethanol, providing nominally 1% by weight of potassium in the combustion products. An MgO-lined run-in section was inserted between the nozzle and the MHD channel to thicken the boundary layer.

The MHD channel used was of a segmented Faraday design, with 13 and 14 electrode pairs in the ABL and IBL series, respectively. The channel was a constant-area channel with MgO sidewalls and insulators and stainless steel electrodes. Optical access was provided by an opening in both channel sidecovers near the downstream end of the channel. The electrode and insulator widths are both 1.9 cm. The channel has a height of 10 cm and a width of 3 cm. The profiles are measured at a location 1.09 m downstream from the nozzle. Current flows in a region 0.45 m long immediately upstream of the measurement point.

### Temperature Diagnostic

During the experiments, plasma temperature profile measurements were made using a modified version of the sodium line-reversal technique.[24] The sodium line-reversal technique is strictly applicable only to equilibrium plasmas. Very near the electrode the electron temperature may be elevated relative to the molecular translational temperature. However, in the region accessible to temperature measurement (>300 $\mu$m from the wall), the electrons should be in equilibrium with the molecules, so the technique is applicable.

In classical line-reversal measurements, the reference lamp temperature is varied until the gas "disappears" when a spectral trace across the sodium line is performed. In our measurement technique, the lamp temperature is fixed and the lamp is alternately blocked and exposed by a chopper. This allows the temperature to be calculated directly from the detector signal. This "generalized line-reversal" temperature measurement scheme is similar to a method used by Vasil'eva.[25]

A gas temperature determination is made by obtaining four radiation intensity signals from the plasma. The four required signals are obtained by recording the intensity of radiation from the plasma with and without a calibrated lamp filament focused in the plasma, at two different optical depths. The lamp on and off conditions are obtained by chopping the lamp and using a simple digital processing scheme to demodulate the signal into the two required signals. The required variation in optical depth is accomplished by using different spectral regions in the wings of a spectral line. The sodium 3*s*-3*p* transition (589.0 nm) was used in the ABL experimental series, and the potassium 4*s*-4*p* transition (767.0 nm) in the IBL experimental series.

The four required signals consist of two signals $P_1$, $P_2$ that see the lamp, and two signals $R_1$, $R_2$ that do not see the lamp. The solution of the radiative transfer equation for the two cases can be expressed as follows:

$$P_i = K[I_b(T_L)e^{-\tau_i} + (1-e^{-\tau_i})\bar{I}_b(T_r)] + n \tag{10a}$$

$$R_i = K(1-e^{-\tau_i})\bar{I}_b(T_r) + n \tag{10b}$$

Here $K$ is an optics calibration factor for the system, $I_b(T_L)$ the blackbody intensity evaluated at the lamp brightness temperature $T_L$ at the wavelength of measurement, $n$ a d.c. bias in the collection system, $\tau_i$ the optical depth of the plasma, and $\bar{I}_b$ the blackbody function evaluated at the plasma reversal temperature. The plasma reversal temperature $T_r$ is defined in a nonuniform plasma by Eq. (13),

$$\bar{I}_b(T_r) = \frac{1}{(e^{\tau}-1)}\int_0^{\tau} I_b(\tau')e^{\tau'}\,d\tau' \tag{11}$$

Here $I_b$ in the integral is evaluated based on the plasma temperature at some location $s$, and $\tau'$ is calculated from the expression

$$\tau'(s) = \int_0^{s} \alpha(s')\,ds' \tag{12}$$

where $\alpha(s')$ is the plasma absorption coefficient evaluated at the measurement wavelength. The four equations have the five unknowns, $K$, $\tau_1$, $\tau_2$, $T_r$, and $n$. One finds that $T_r$ can be determined from the four equations, even though the other variables cannot. The expression for $T_r$ is

$$T_r = \frac{hc/\lambda k}{\left[\dfrac{hc/\lambda k}{T_\ell} + \ell n\left(1+\dfrac{P_1-P_2}{R_2-R_1}\right)\right]} \tag{13}$$

Here $h$ is Planck's constant, $c$ the speed of light, $\lambda$ the wavelength of light used in the measurement, and $k$ the Boltzmann gas constant.

Because of the existence of cool sidewall boundary layers, it is necessary to apply a correction to the measured temperature. As all of the measurements were taken with an optical depth less than unity, we can estimate the effect of boundary layers on the measurement by assuming that the measured $\bar{I}_b$ is equal to the spatial average of $I_b$.[13] The boundary-layer correction is performed by assuming a power law form for the sidewall temperature profile. As the sidewall boundary layers have met, the assumed functional form for the gas temperature $T$ consists of two identical boundary layers of thickness $L/2$ (where $L$ is the optical path length through the gas),

$$s<\frac{L}{2}, \quad T = T_w + (T_c - T_w)\left(\frac{s}{L/2}\right)^{1/N}$$

$$s>\frac{L}{2}, \quad T = T_w + (T_c - T_w)\left(\frac{L-s}{L/2}\right)^{1/N} \tag{14}$$

Here $T_c$ is the core temperature and $T_w$ the wall temperature. The values of $T_w$ and $N$ are estimated, partially on the basis of measurements and partially from calculations, to be $T_w = 2000$ K and $N = 9$. Given the model temperature profile, the boundary-layer correction is applied by estimating a value of $T_c$, calculating the spatial average of $I_b$ using the model

temperature profile, and iterating on $T_c$ until the calculated spatial average of $I_b$ is equal to the measured quantity $\bar{I}_b$. The resulting $T_c$ is the corrected plasma temperature for a particular measurement.

Uncertainties in the sidewall correction introduce an absolute uncertainty in the temperature of about ±25 K, and a relative uncertainty among the various temperatures at different points in a boundary-layer measurement of about 15 K. The total estimates for uncertainty, including the uncertainty in the sidewall correction, are ±50 and ±75 K for the absolute error in the ABL and IBL experiments, respectively, and ±25 K for the relative error in both sets of experiments.

A diagram of the optical setup used in the IBL series of experiments is shown in Fig. 2. The optical setup for the ABL experiments is similar, but somewhat simpler since the channel in the ABL experiments was not in the magnetic field. Further details of the optical design and the diagnostic are available in James.[13]

The temperature measurements were typically performed over an electrode, with an axial spatial resolution of the order of several millimeters. In the IBL experiments temperature profiles were measured at various axial locations along an electrode-insulator cycle, but only minor variations in the profiles were observed, even at relatively high current levels. We therefore believe that local hot spots do not affect the measurements.

## Experimental Results and Interpretations

### Profile Measurements with No MHD Effects

One of the principal difficulties encountered in modeling boundary layers in MHD generators is the modeling of the plasma flow without any MHD effects such as Joule heating or magnetic field interactions. The non-MHD flow involves turbulent boundary layers with large density gradients, moderate Mach numbers, variable properties, possibly rough surfaces, combustion fluctuations, etc. The first results presented therefore will be for profiles measured in the absence of MHD effects.

Because of the inherent uncertainties that exist in the experimental conditions, it is necessary to vary one or more free parameters in the theoretical calculations to match the calculations to the data. The free parameter used in the calculations is the initial plasma temperature at the nozzle exit. In matching theoretical calculations to data, the initial plasma temperature was adjusted until the calculated temperature at the edge of the boundary layer matched the measured temperature at the same location. This adjusted core temperature is typically within 50-100 K of the expected temperature based on heat balances from previous experiments.

Wall boundary conditions were obtained from thermocouple measurements of the MgO and electrode surface temperatures. Average values for the surface temperatures for conditions without current are:

ABL Runin (0-0.62 m): $T$ varies approximately linearly with $x$ from 2200-1900 K; channel (0.62-1.09 m): $T = 1300$ K.

IBL Runin: As in ABL; channel: $T = 1450$ K.

Based on these temperatures, a heat-transfer coefficient $H$ for heat transfer from the surface to coolant at 300 K was established using the boundary-layer calculation. For cases with current, $H$ was kept constant, allowing the electrode temperature to rise when current was applied in the calculation.

Comparison of data and theory is shown in Fig. 3. The data displayed were chosen to span a variety of run conditions and experimental days (with $J=0$, $B=0$). Descriptions of the run conditions may be found in Table 1. The theoretical calculation uses standard values of the turbulence constants, i.e., $\kappa = 0.41$, $A_0^+ = 25.0$, and $A_c = 0.005$.

The graphs show that there was generally adequate agreement between the experimental profiles and theoretical calculations based on standard values of the turbulence constants. Some small differences between data and theory are seen in the data very near the wall and in the overall shape of the profiles, but these differences are not felt to be significant.

Calculations were performed in which the turbulence constants $\kappa$, $A_0^+$, and $A_c$ were varied from their accepted values. In addition, the turbulence model was modified to account for roughness effects using the model suggested by Healzer[26] and the sand grain roughness parameter was varied. Modifications of the parameters did not improve the fit of the data to the theory. The same procedure was applied to the data of Rankin.[9] Rankin measured a velocity profile on the insulating wall of the Stanford M-2 channel under conditions similar to those of the present experiments. As shown in Fig. 4, the best fit of theory to his data was obtained when the value of $A_c$ was changed from its usual value of 0.005 to 0.010, while all of the other parameters took on their accepted value and zero roughness was used.

The increase of $A_c$ from 0.005 to 0.010 is a method of modeling the effect of large core turbulence. The measurements of Rankin did show a large value of turbulence compared to measurements in normal pipe flows. Rankin measured the value of

$$\frac{(\overline{u'^2})^{1/2}}{u_\infty} \tag{15}$$

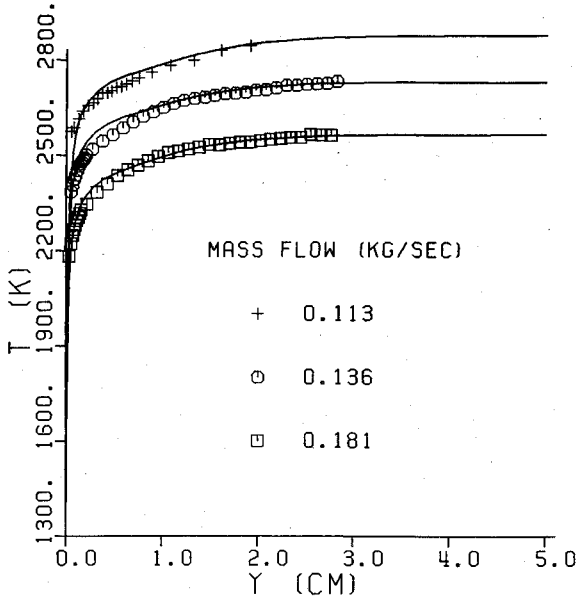


**Fig. 3 Comparison of data to theory for cases with no MHD effects; data are from runs I4310 (pluses), A3535 (circles), and A2360 (squares).**

**Table 1 Summary of conditions for experimental runs**

| Run No.[a] | $\dot{m}$, kg/s | N/O (by mass) | $u_\infty$,[b] m/s | $T_\infty$,[b] K | $B$, T | $\bar{J}_y$,[c] A/cm$^2$ |
|---|---|---|---|---|---|---|
| A2360 | 0.181 | 1.00 | 425 | 2550 | 0 | 0 |
| A3410 | 0.136 | 0.50 | 350 | 2700 | 0 | 0 |
| A3465 | 0.136 | 0.50 | 350 | 2700 | 0 | −1.51 |
| A3535 | 0.136 | 0.50 | 350 | 2700 | 0 | 0 |
| I3410 | 0.158 | 0.50 | 405 | 2700 | 0 | 0 |
| I3421 | 0.158 | 0.50 | 405 | 2700 | 0 | 0.95 |
| I3430 | 0.158 | 0.50 | 405 | 2700 | −1.8 | 0.65 |
| I4310 | 0.113 | 0.00 | 325 | 2850 | 0 | 0 |
| I4330 | 0.113 | 0.00 | 325 | 2850 | 1.8 | −0.95 |

[a] Prefix A corresponds to the ABL run series, and I to the IBL run series.
[b] $u_\infty$ and $T_\infty$ are nominal values for conditions at the nozzle exit.
[c] Current density based on the core area. Measured boundary layer was on the anode wall for negative $\bar{J}_y$ and cathode wall for positive $\bar{J}_y$.

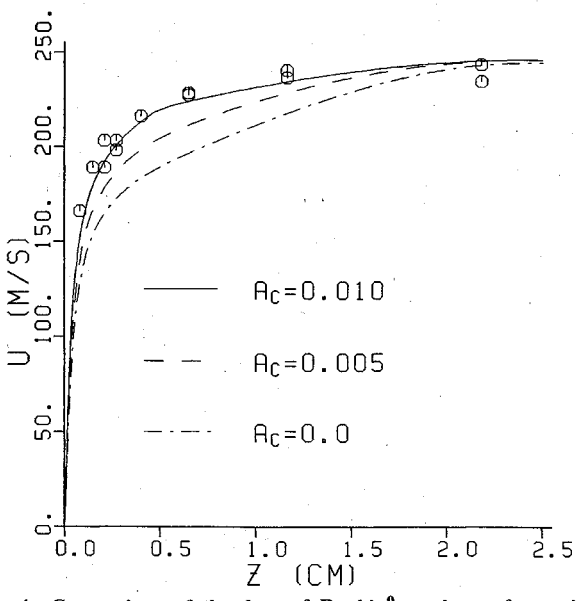


Fig. 4 Comparison of the data of Rankin[9] to theory for various values of the freestream turbulence parameter $A_c$.

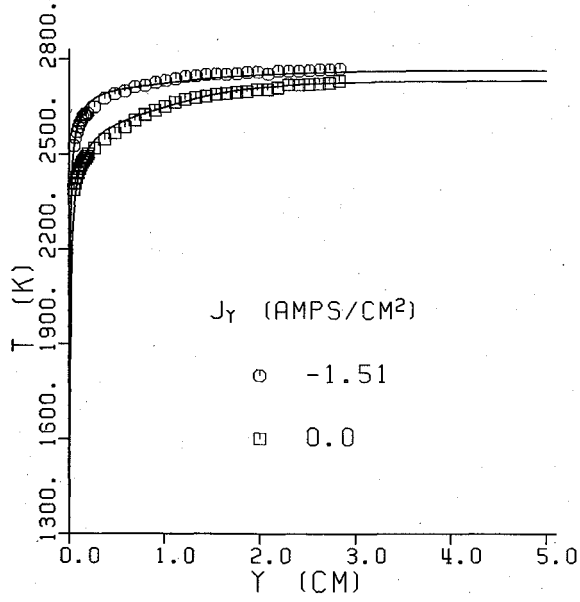


Fig. 5 Comparison of data to theory for the effect of Joule heating on an anode boundary layer; data are from runs A3410 (squares) and A3465 (circles).

obtaining ~6% at the channel centerline. Laufer's measurements[27] of the same quantity in pipe flow gave a value of ~3%. Increasing $A_c$ seems therefore to be justified by the core turbulence measurements. Large core turbulence seems to be a reasonable and consistent explanation for the difficulties encountered by Rankin in matching his data to theory.

The source of the discrepancy between the value of $A_c$ needed to fit the present data and the data of Rankin is not known. Research is required on the effects of freestream turbulence, which is modeled by $A_c$, on MHD boundary layers. For the purpose of this work, further comparisons of data to theory use the standard values for the turbulence constants, including $A_c = 0.005$. This value of $A_c$ should not be extrapolated to calculations involving large channels without careful consideration, as the scale of freestream turbulence that will occur in a large generator is not presently known, and may not be properly modeled by the simple freestream turbulence model employed here.

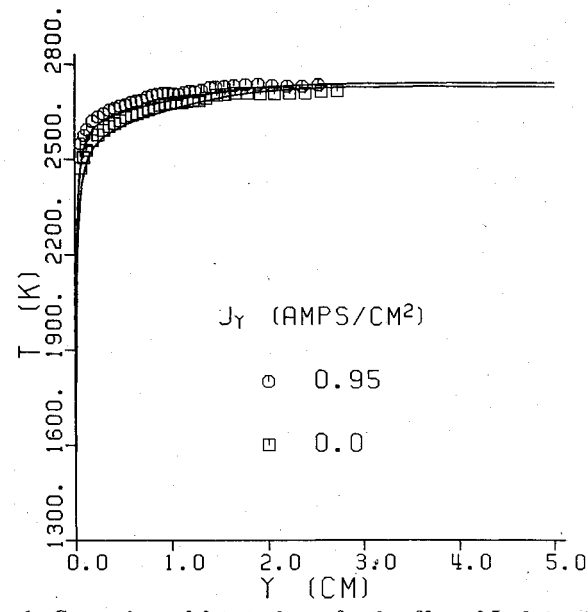


Fig. 6 Comparison of data to theory for the effect of Joule heating on a cathode boundary layer; data are from runs I3410 (squares) and I3421 (circles).

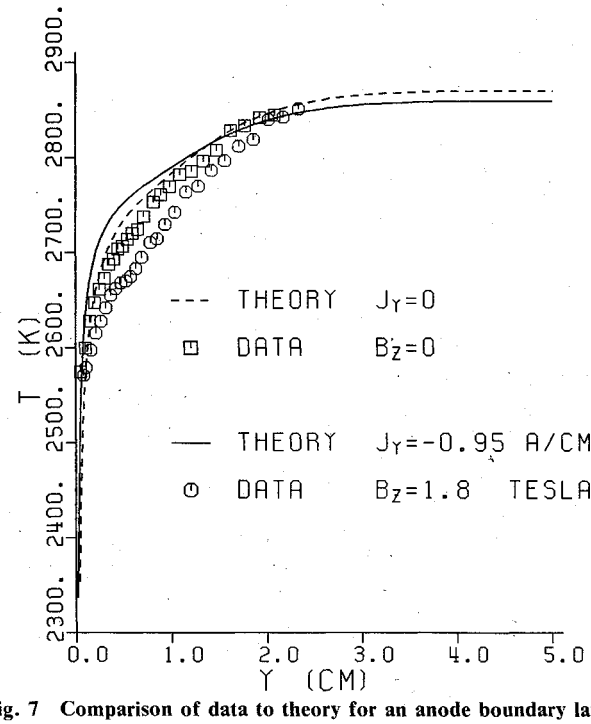


Fig. 7 Comparison of data to theory for an anode boundary layer with magnetic field; data are for runs I4310 (squares) and I4330 (circles).

### Joule Heating Effects on Temperature Profiles with No Magnetic Field

When current flows through the electrode wall boundary layer, Joule heating causes an increase in the temperature of the plasma throughout and a thinning of the enthalpy boundary layer. Several sets of temperature profiles were measured that show this effect. These measurements require comparison of a temperature profile measured without current to a profile measured with current. Typically the temperature profile was first measured without current, then current was applied, and the profile was measured with current.

Theoretical calculations of the boundary layers with and without current were made and compared with the data. The

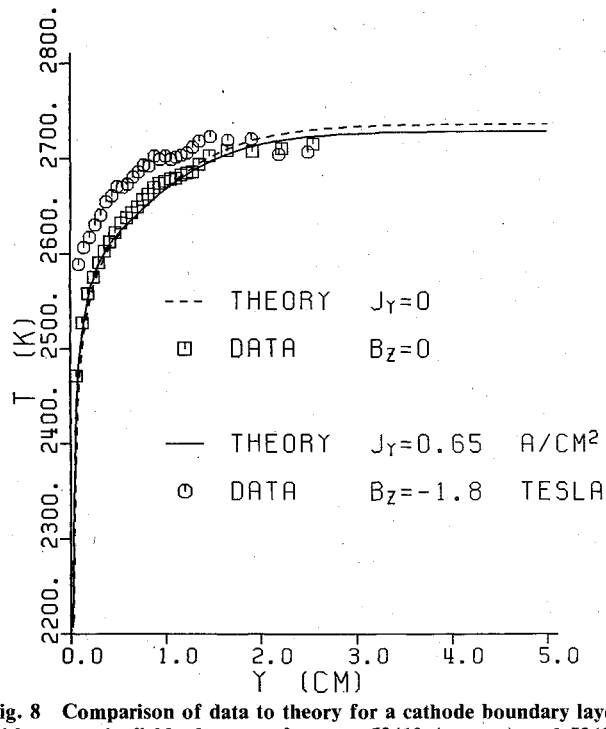


**Fig. 8 Comparison of data to theory for a cathode boundary layer with magnetic field; data are for runs I3410 (squares) and I3430 (circles).**

calculations use the standard values of the turbulence constants. The average core current density from the experimental runs is used to specify the current density in the calculation, with a correction for the effect of the sidewall boundary layers, described in James.[13]

Comparisons of data and theory for two runs are shown in Figs. 5 and 6. The data were taken in both the IBL and ABL experimental series at two different flow settings and include both anode and cathode boundary layers. The theoretical profile for the no-current case is matched with the no-current data by varying the inlet temperature in the theory. The theoretical profile for the case with current is calculated using the same parameters as for the case without current, except that the current density is set to the experimentally measured current density value corrected for sidewall boundary-layer effects.

The general agreement between theory and data is excellent. The magnitude of the temperature increase due to Joule heating is calculated quite well. Minor discrepancies that occur between data and theory appear to be a result of inadequacies in modeling the profiles without current. The theoretical agreement is equally good for both anode and cathode boundary-layer profiles.

#### Profile Measurements with Current and Magnetic Field

In the IBL series of experiments, temperature profiles were measured under conditions with current and with a magnetic field of 1.8 T. The temperature profiles under these conditions, in addition to being affected by Joule heating, are influenced by the magnetic field both through the energy-removal term $J_y uB$ in the energy equation and through the $\boldsymbol{J}\times\boldsymbol{B}$ terms in the momentum equation. In the $x$ momentum equation, the effect of the $\boldsymbol{J}\times\boldsymbol{B}$ force should be canceled exactly by the pressure gradient. However, current nonuniformities in the $x$ and $z$ direction can lead to changes in the velocity field due to magnetic field effects in the $y$ and $z$ momentum equations. Such effects are not modeled by the two-dimensional boundary-layer theory in the present work.

The temperature profiles were obtained in a sequence similar to that used in the experiments without magnetic field. The profile was measured first without current or magnetic field, second with current applied but without magnetic field, and finally with magnetic field and current.

A comparison of theoretical predictions to data with magnetic field is shown in Figs. 7 and 8. The calculation without current is matched to the data by varying the inlet temperature. The calculation with current and magnetic field is performed using the same conditions as the calculation without current, except that the experimental values of magnetic field and current density (corrected for sidewall effects, as described in Ref. 13) are applied.

The theory and data show noticeable disagreement in the presence of a magnetic field. The theory predicts that the effect of current and magnetic field is to lower the temperature in the core and raise the temperature near the wall. The temperature variation is caused by the term

$$(J^2/\sigma) + J_y uB_z \tag{16}$$

which appears in the energy equation. The term is negative in the core and positive near the wall due to the lower values of $\sigma$ and $u$ near the wall. In contrast, the temperature data with current and magnetic field are generally lower than the data without current for the anode boundary-layer measurement of Fig. 7, and higher for the cathode boundary-layer measurement of Fig. 8. Further examples of such behavior were seen in other measured profiles.

The effect of magnetic field on the data may be explained by the influence of nonuniformities in the $z$ direction on the $x$-directed current. In our experiments, measurements of $E_x$ for cases with the magnetic field generally showed that $E_x$ had a value approximately half that required to suppress the flow of axial current in the core. This reduction in $E_x$ may be due to current leakage through the metal sidewalls. The lowered Hall voltage results in a net $x$-directed current $J_x$ induced by the Hall effect. Because of cool insulating wall boundary layers, the magnitude of $J_x$ is larger in the core than in the insulating wall boundary layer. The effect of this $J_x$ variation in the $x$-$z$ plane is to induce a force variation in the $y$-$z$ plane that is not balanced by pressure forces. This force variation induces a secondary flow in the $y$-$z$ plane, pushing the cool fluid from the insulating wall boundary layer into the anode boundary layer and the hot core fluid into the cathode boundary layer. The net effect is a cooling of the anode boundary layer and a heating of the cathode boundary layer. Such recirculations have been predicted theoretically by Maxwell et al.[28]

The magnitude of $J_x$ in the core of the channel was estimated based on measurements performed with voltage pins. The core $J_x$ is generally about one-third to one-half of the core $J_y$. Using this $J_x$, the magnitude of the secondary flow can be estimated from a momentum balance to be of the order of 30 m/s. This velocity is about 7% of the freestream velocity and could certainly cause an effect of the magnitude observed in the data.

## Conclusions

Experimental measurements were performed of temperature profiles on a laboratory-scale MHD generator. Comparisons between calculations from the two-dimensional theory and measurements for cases without current generally showed good agreement when the turbulence model properly accounted for effects of freestream tubulence. Comparisons of experimental temperature profiles without current to profiles with current showed a marked temperature increase in the boundary layer due to Joule heating. The magnitude of the increase was well predicted by the two-dimensional boundary-layer theory. Measured temperature profiles with current and magnetic field did not agree with predictions. The predicted profile in the inner region of the boundary layer for a case with current and magnetic field was above a similar case without current, whereas measurements for anode boundary layers were below control profiles without current.

A cathode boundary layer behaved oppositely to the anode boundary layers. It is suggested that three-dimensional recirculation induced by nonuniformities in axial current may explain the discrepancies.

## Acknowledgment

This research was supported by the U.S. Department of Energy under Contract EX 76-C-01-2341 and National Science Foundation Grant AER-72-03487.

## References

[1] Kerrebrock, J. L., "Electrode Boundary Layers in Direct-Current Plasma Accelerators," *Journal of the Aerospace Sciences*, Vol. 28, No. 8, 1961, p. 631.

[2] Hale, F. J. and Kerrebrock, J. L., "Insulator Boundary Layers in Magnetohydrodynamic Channels," *AIAA Journal*, Vol. 2, March 1964, p. 461.

[3] High, M. D. and Felderman, E. J., "Turbulent MHD Boundary Layers with Electron Thermal Nonequilibrium and Finite Rate Ionization," *AIAA Journal*, Vol. 10, Jan. 1972, pp. 98-103.

[4] Sherman, A., Hsuan, Y., Reshotko, E., and McAssey, E., Jr., "MHD Boundary Layers with Non-equilibrium Ionization and Finite Rates," AIAA Paper 71-139, 1971.

[5] Doss, E. D., Dwyer, H. A., and Hoffman, M. A., "Influence of Segmentation and Ambipolar Diffusion on MHD Non-equilibrium Boundary Layers," *AIAA Journal*, Vol. 12, Feb. 1974, pp. 155-162.

[6] Cott, D. W., "Ionizational and Electron Thermal Nonequilibrium in MHD Boundary Layers," *AIAA Journal*, Vol. 9, Dec. 1971, pp. 2404-2410.

[7] Argyropoulos, G. S., Demetriades, S. T., Doss, E. D., and Oliver, D. A., "Electron Nonequilibrium in Open Cycle MHD Generators," *AIAA Journal*, Vol. 12, May 1974, pp. 669-671.

[8] Daily, J. W., Kruger, C. H., Self., S. A., and Eustis, R. H., "Boundary Layer Profile Measurements in a Combustion Driven MHD Generator," Paper presented at Sixth International Conference on MHD Electrical Power Generation, Washington, D.C., June 1975; also *AIAA Journal*, Vol. 14, Aug. 1976, pp. 997-1005.

[9] Rankin, R. R., Self, S. A., and Eustis, R. H., "Study of the Insulating Wall Boundary Layer in a Faraday MHD Generator," *AIAA Journal*, Vol. 18, Sept. 1980, pp. 1094-1100.

[10] Demetriades, S. G., Argyropoulos, G. S., and Maxwell, C. D., "Progress in Analytical Modeling of MHD Power Generators," Paper presented at 12th Symposium on Engineering Aspects of MHD, Argonne, Ill., 1972.

[11] Kessler, R., "Effects of Electrode Temperature on MHD Generator Performance," Institute for Plasma Research, Stanford University, Stanford, Calif., SUIPR Rept. 239; also AFAPL-TR-67-77, June 1968.

[12] Kirillov, V. V., Semenov, V. D., and Yundev, D. N., "Measurement of the Temperature Distribution in a Boundary Layer at the Channel Walls of an Open Cycle MHD Generator," *High Temperature*, Vol. 11, No. 6, 1973, pp. 1181-1182.

[13] James, R. K., "Joule Heating Effects in the Electrode Wall Boundary Layer of MHD Generators," U.S. Dept. of Energy Rept. FE-2341-15; also Ph.D. Thesis, Stanford University, Stanford, Calif., Jan. 1980.

[14] Martinelli, R. C., *Transactions of the ASME*, Vol. 69, 1947, p. 947.

[15] Crawford, M. E. and Kays, W. M., "STAN5—A Program for Numerical Computation of Two-Dimensional Internal/External Boundary Layer Flows," Mechanical Engineering Dept., Stanford University, Stanford, Calif., Rept. HMT-23, 1975.

[16] Hinnov, E. and Hirschberg, J. G., "Electron-Ion Recombination in Dense Plasmas," *Physics Review*, Vol. 125, 1962, pp. 795-801.

[17] Kelley, R. and Padley, P. J., "Measurement of Collisional Ionization Cross-Sections for Metal Atoms in Flames," *Proceedings of the Royal Society of London*, Ser. A, Vol. 327, 1972, pp. 345-366.

[18] Pepper, J. W., "Effect of Nitric Oxide Control on MHD-Stream Power Plant Economics and Performance," Institute for Plasma Research, Stanford University, Stanford, Calif., Rept. SUIPR 614, May 1974.

[19] Spencer, F. E. and Phelps, A. V., "Momentum Transfer Cross-Sections and Conductivity Integrals for Gases of MHD Interest," Paper presented at 15th Symposium on Engineering Aspects of MHD, Philadelphia, Pa., 1976.

[20] Mitchner, M. and Kruger, C. H., *Partially Ionized Gases*, John Wiley & Sons, New York, 1973, Chap. 3.

[21] Clement, R. M., "Some Measurements of the Ion Current to a Spherical Probe in an Atmospheric Pressure Combustion MHD Plasma," *Combustion and Flame*, Vol. 25, 1975, pp. 393-395.

[22] Oliver, D. A., "Nonuniform Electrical Conduction in Magnetohydrodynamic Channels," Institute for Plasma Research, Stanford University, Stanford, Calif., Rept. SUIPR 168, May 1967.

[23] Reseck, K. G., "Performance Characteristics of a Combustion-Driven MHD Power Generator," Institute for Plasma Research, Stanford University, Stanford, Calif., Rept. SUIPR 76, Aug. 1966.

[24] Strong, H. M. and Bundy, F. P., "Measurement of Temperatures in Flames of Complex Structure by Resonance Line Radiation: I. General Theory and Application to Sodium Line-Reversal Methods," and "Measurement of Temperatures in Flames of Complex Structure by Resonance Line Radiation: II. Sodium Line Reversal by High-Resolution Spectroscopy," *Journal of Applied Physics*, Vol. 25, Dec. 1954, pp. 1521-1537.

[25] Vasil'eva, I. A., Kirillov, V. V., Maksimov, I. A., Malyuzhonok, G. P., and Novosadov, V. B., "Measurement of a Plasma's Temperature by a Spectroscopic Method with Continuous Automatic Detection," *High Temperature*, Vol. 11, No. 4, July-Aug. 1973.

[26] Healzer, J. M., Moffat, R. J., and Kays, W. M., "The Turbulent Boundary Layer in a Rough, Porous Plate: Experimental Heat Transfer with Uniform Blowing," Dept. of Mechanical Engineering, Stanford University, Stanford, Calif., Rept. HMT-18, 1974.

[27] Laufer, J., NACA TR 1174, 1954.

[28] Maxwell, C. D., Markham, D. M., Demetriades, S. T., and Oliver, D. A., "Coupled Electrical and Fluid Calculations in the Cross Plane in Linear MHD Generators," Paper presented at 16th Symposium on Engineering Aspects of MHD, University of Pittsburgh, Pa., 1977.